

Calibration of the absolute light–yield of various scintillator screens for electron bunch charge determination in laser–plasma accelerators

Thomas Kurz,^{1,2,3,a)} Jakob Matthias Krämer,^{1,3} Jurjen Pieter Couperus,^{1,3} Hao Ding,^{2,4} Stefan Kuschel,^{5,6} Alexander Köhler,^{1,3} Omid Zarini,^{1,3} Dominik Hollatz,^{5,6} David Schinkel,^{5,6} Richard D’Arcy,⁷ Jan Patrick Schwinkendorf,^{7,8} Arie Irman,¹ Ulrich Schramm,^{1,3} and Stefan Karsch^{2,4}

¹⁾ *Helmholtz–Zentrum Dresden–Rossendorf, Bautzner Landstraße 400, D-01328 Dresden, Germany*

²⁾ *Ludwig–Maximilians–Universität München, Am Coulombwall 1, D-85748 Garching, Germany*

³⁾ *Technische Universität Dresden, D-01069 Dresden, Germany*

⁴⁾ *Max–Planck–Institut für Quantenoptik, Hans–Kopfermann–Straße 1, D-85748 Garching, Germany*

⁵⁾ *Helmholtz–Institut Jena, Fröbelstieg 3, D-07743 Jena, Germany*

⁶⁾ *Friedrich–Schiller–Universität Jena, Fürstengraben 1, D-07743 Jena, Germany*

⁷⁾ *Deutsches Elektronen–Synchrotron, Notkestraße 85, D-22607 Hamburg, Germany*

⁸⁾ *Universität Hamburg, Jungiusstraße 9, D-20355 Hamburg, Germany*

(Dated: 22 July 2017)

This article gives information about the absolute light yield of different scintillating screens used in current laser-plasma experiments. The calibration was designed to investigate the light/charge–conversion and saturation effects of different screens. In order to reach the necessary electron fluence, the screens were excited by a focused electron beam, generating high peak charge density up to 20 nC/mm² delivered from the ELBE linear accelerator at the Helmholtz Center in Dresden–Rossendorf. A three orders of magnitude linearity in light yield to charge conversion was found followed by a saturation area starting in the range of nC/mm². Furthermore for a specific type of scintillator long–term stability test were done. A significant decrease of the scintillation efficiency with conditions comparable to a LPA–experiment was found. Also included is a description for a new type of reference light source performing the screen cross–calibration.

Usage: Secondary publications and information retrieval purposes.

PACS numbers: May be entered using the `\pacs{#1}` command.

Structure: You may use the `description` environment to structure your abstract; use the optional argument of the `\item` command to give the category of each item.

PACS numbers: Valid PACS appear here

I. INTRODUCTION

Since their theoretically predication in 1979 by Tajima and Dawson¹, laser-plasma wakefield accelerators (LWFA) have seen tremendous progress. These accelerators can operate with accelerating gradients of up to several hundreds of GeV m^{−1}, three to four orders of magnitude higher than in conventional accelerators. Recent advancement in both the understanding of the acceleration mechanism as well as development of state of art laser–systems, which are now able to operate in the petawatt–regime^{2,3}, make it possible to accelerate quasi-monoenergetic^{4–6} electron bunches containing charges of several hundred pC to energies in the GeV–range^{7–9}. Providing ultra–short bunch lengths of only a few femtoseconds, these accelerators can deliver several tens of kA peak-current^{10?} making them ideal drivers for next-generation compact light-sources covering high-field THz[?]?, high-brightness X-ray^{11,12} and γ -ray^{13,14}

sources, compact FELs^{15?–18} and laboratory-size beam-driven plasma accelerators^{19,20}.

However, laser plasma accelerators (LPAs) are still a developing field. Compared to conventional accelerators many challenges remain, both in beam quality as well as in shot-to-shot stability. In order to further improve the performance of LPAs, it is necessary to understand the accelerator dynamics and to be able to resolve shot-to-shot fluctuations. Therefore, a well suited single-shot electron diagnostic is required which resolves charge, energy and divergence over a large parameter range.

Typically a combination of a broad energy-range dipole magnet, which maps electron energy to position in the dispersive plane, is used in combination with a scintillation screen imaged onto a camera for charge diagnostic. This screen generally covers an area in the order of hundreds of cm² in order to cover the relevant parameter range. Established techniques at conventional accelerators such as Faraday cups and integrating current transformers (ICT) aren’t reasonable alternatives, as they are not capable of delivering the required energy–resolved charge information.

^{a)} E-Mail adress: t.kurz@hzdr.de

These scintillation screens consist of a $10\mu\text{m}$ to $100\mu\text{m}$ -thick layer of powdered rare earth phosphor ($\text{Gd}_2\text{O}_2\text{S:TB}$), that converts the electron energy into visible light. The process is dominated by fluorescence and has a life-time of approximately 1 ms. This short life-time enables single shot diagnostic at relevant LPA repetition rates (up to 10 Hz). In contrast, imaging plates, which deliver good energy resolution and a high dynamic range^{21–24}, suffer from a long read-out time. Scintillating screens are commercially available, often under the trade name LANEX, and marketed for X-ray detection. Generally no electron-photon conversion efficiency is specified and careful calibration is required before application.

In this work we report on the absolute charge calibration of several commercially available scintillating screens. These calibrations are performed under conditions close to those found in LWFA experiments, providing a significant improvement over previous reported calibration values by Buck et al.²⁵. Additionally we report on several other relevant effects. In section III A 2 the non-linear response of the scintillator at high electron flux is presented. Crucial information on the long term stability and damage resistivity of the screens are reported in section III B.

The insights found in this work will have a significant impact on the application of scintillating screens as a charge diagnostic at LPAs. The absolute calibration presented here has significant improvements compared to previous work and will act as a new standard in the field.

II. EXPERIMENTAL SETUP

The setup for the absolute charge calibration of the scintillation screens is illustrated in Fig. 1. The measurement was performed at the ELBE linear accelerator (LINAC) at the Helmholtz-Zentrum Dresden-Rossendorf. The accelerator was operated such that it produced sub-10 ps long electron bunches with charges up to 50 pC and a maximum kinetic energy of 23 MeV at 13 MHz repetition rate. For generating higher charges, the accelerator changed into multiple bunch mode. This means the cavity emits a train of pulses that is tunable in its length. The temporal delay of the single bunches within this pulse-train is 77 ns. All these short bunches add their charge onto the screens, due to the short delay compared to the lifetime of the excited state ($\approx 1\text{ ms}$) in the scintillator²⁶. The electron beam emitted by the LINAC is focused by magnetic quadrupoles to a focal spot. This leads to a FWHM-beam size of 6 mm^2 to 7 mm^2 at the target. This small spot size enabled us to reach charge densities up to 20 nC/mm^2 which are necessary to study saturation effects in the active layer of the scintillator. In front of the screen, the charge of the focused electron bunch is measured by an integrated current transformer (ICT-082-070-05:1-VAC, Bergoz Instrumentation, France). In order to get a useful ICT signal the pulses were amplified (Pulse Amplifier Coax-

ial ZPUL-30P, Mini Circuits, USA) by roughly a factor of 50 and recorded by a high quality oscilloscope (Information required). Simulations show that the energy deposition of the electrons inside the photo-luminescent layer is almost independent of their kinetic energy above a threshold-value of 3 MeV^{22,27,28}. Thus the calibration results can be used to determine the charge in an experiment with highly relativistic electrons, i.e. laser wakefield acceleration even though the energy is one order magnitude lower than in LPA experiments. After passing the ICT, the electrons collide with the screen. The screens were mounted on a rotating target wheel which was aligned $(22 \pm 1)^\circ$ relative to the electron beam. This geometry enables us to mount the deflector mirror out of the beam-axis and therefore avoid any optical transition radiation (OTR) background. In the active layer of the screen, phosphor atoms get excited by the incoming electrons which radiate photons while relaxing back into the ground state. The light emission distribution of these screens follows approximately Lambertian law²⁹. The emitted photons with a peak wavelength λ_{peak} of 546 nm are reflected by a silver mirror (Thorlabs, PF20-03-P01) under $(34 \pm 1)^\circ$ to a 12-bit CCD-camera (Basler, acA1300-30gm) equipped with a high-definition tele-objective imaged to the CCD-chip. Thanks to the alignment of the mirror the camera looks perpendicularly onto the screens which maximizes the light emission onto the CCD-chip according to Lambertian law. In front of the camera-lens, another ND-filter wheel ranging from ND0.5 to ND4.0 is placed for generating a dynamic range containing 7 orders of magnitude. The ND-filters are an important component because they are used directly (part of β in eq. 1) in the calibration run to adapt the screen's signal to the dynamic range of the CCD-camera as well as in the quantum efficiency measurement of the CCD-chip. Thus the filters were calibrated precisely using a well-calibrated photo-spectrometer (Cary[®] 50 UV-VIS). Additionally an optical fiber (M200L02S-A, Thorlabs) connected to a spectrometer (HR4000, Ocean Optics) is implemented in the setup in order to determine the spectrum of the scintillation screens and the constant light sources. The fiber is placed on a linear motor to switch quickly between calibration and spectrum measurements.

III. RESULTS

A. Absolute charge calibration

We have calibrated our optical detection system in order to calculate the absolute amount of photons/sr emitted by the the scintillator. Together with a precise knowledge (5% accuracy) of the LINAC's bunch charge we are able to determine the absolute scintillation efficiency (photons/e⁻) in case of an excitation with relativistic electrons. The effective aperture in our optical detection system was defined by the diameter of a one-

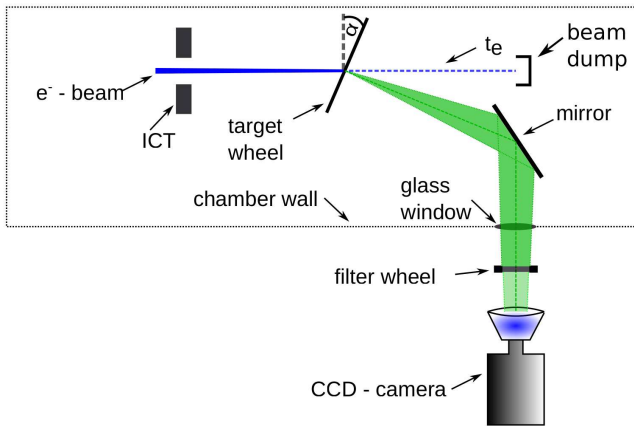


FIG. 1. Setup for absolute charge calibration of scintillation screens: ICT measures the charge of the electron beam. Six different screens with an angle of 22° relative to the incoming electron beam are mounted on a filter wheel and imaged via a silver mirror onto a CCD-chip. In order to generate the desired dynamic range a set of ND-filters were placed in front of the camera.

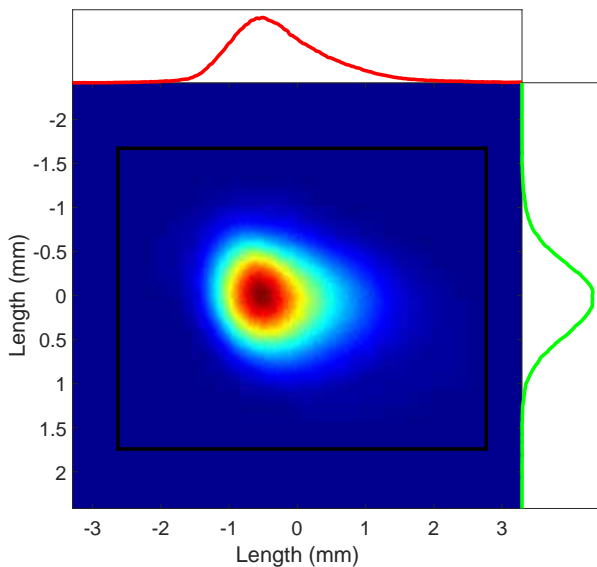


FIG. 2. Image of electron bunch recorded by CCD-sensor. The rectangle marks the region of interest (ROI) only this area was used for the analysis. The two curves indicate the line—out of the electron bunch through its peak in horizontal and vertical dimension. The area of the bunch at FWHM is $\approx 6 \text{ mm}^2$.

inch large aperture. It was mounted at a distance of $(361 \pm 4) \text{ mm}$ to the target. The diameter was measured to be $(22.96 \pm 0.05) \text{ mm}$ resulting in a collection angle of $(2.89 \pm 0.07) \times 10^{-3} \text{ sr}$. A representative image of an electron bunch that was recorded by the CCD-chip during the calibration is shown in Fig. 2. For the analysis of the brightness of the scintillator, the CCD-counts of

this image are summed up and the camera background as well as the accelerator background (darkcurrent) is subtracted. Therefore, the number of photons N_{photon} emitted by the scintillator into a surface covering one steradian per amount of incident electrons N_{electron} can be described as

$$\frac{N_{\text{photon}}}{N_{\text{electron}}} = N_{\text{count}} \cos(\theta) \beta^{-1} \Omega^{-1} N_{\text{electron}}^{-1}, \quad (1)$$

where N_{count} describes the number of counts summed up over the ROI of the raw image. θ is the orientation of the electron beam and normal vector of the scintillator's surface. Thus the photon signal recorded by the CCD-camera was corrected to the incidence angle of the electrons. β denotes the efficiency of the entire detection system, i.e. the probability for a photon created at the source, traveling through the optical beamline, reaching the CCD-chip and finally being converted to a binary number by the ADC. Finally Ω symbolizes the effective collection angle in units of steradian. For completeness, β can be disassembled in its individual parts. The transmission of the off-axis mirror at the specific wavelength is $(97 \pm 1) \%$, the window of the vacuum-chamber transmits $(91.3 \pm 0.5) \%$ of the incoming light and the objective images 88 ± 1 out of 100 impinging photons on the the chip. Furthermore the photon-to-count conversion efficiency of $(32.8 \pm 1.7) \%$ of the CCD-chip (Sony ICX445) and its associated readout-electronics have been determined precisely using well-calibrated ND-filters to adapt the photon flux from a green laser.

The response functions for the different screens are shown in Fig. 3. The curves show a linear behavior until an upper boundary caused by saturation and degeneration effects (Sec. III A 2, III B). In order to determine the calibration value for the absolute response of the different scintillator, a linear fit has been applied to all datapoints within the linear region. The resulting calibration values are shown in TABLE I. The error of the values was determined using the method of Gaussian error propagation.

1. Cross-calibration

In order to simplify the determination of the charge in a laser-plasma experiment based on the result of this calibration experiment, additionally reference light sources were recorded by the CCD-camera. As long as the reference source delivers a constant photon signal over time and the calibration was performed with identical geometrical parameters (ensured by the filter-wheel in our case) the relative signal between the screen and the reference light source became independent of the detector geometry. In particular, we implemented a gaseous tritium light source (GTLS) and an LED-based diffused green radiator. The LED-source is aimed for an extended life time because it is operated by a constant current source with current fluctuation below 1%. Fortunately, the source

TABLE I. Calibration values for different scintillation screens: The absolute light yield per incident electrons (first column) and the saturation threshold as well as the resulting fitting parameter (middle and right column).

Screen	Absolute fluorescence efficiency (10^9 ph/sr/pC)	Saturation threshold (10^3 pC/mm ²)	Birk's constant (10^{-5} mm ² /pC)
KODAK BioMAX	7.67 ± 0.42	4.2 ± 0.2	5.9 ± 0.3
Cawo OG B	5.81 ± 0.32	5.0 ± 0.3	5.0 ± 0.3
Cawo OG F	3.70 ± 0.26	4.9 ± 0.3	5.1 ± 0.3
Konica Minolta OG 400	3.67 ± 0.18	5.2 ± 0.4	4.8 ± 0.4
Carestream Lanex Regular	3.10 ± 0.15	5.1 ± 0.3	4.9 ± 0.3
Kodak Lanex Fine	0.96 ± 0.06	9.6 ± 0.5	2.6 ± 0.3

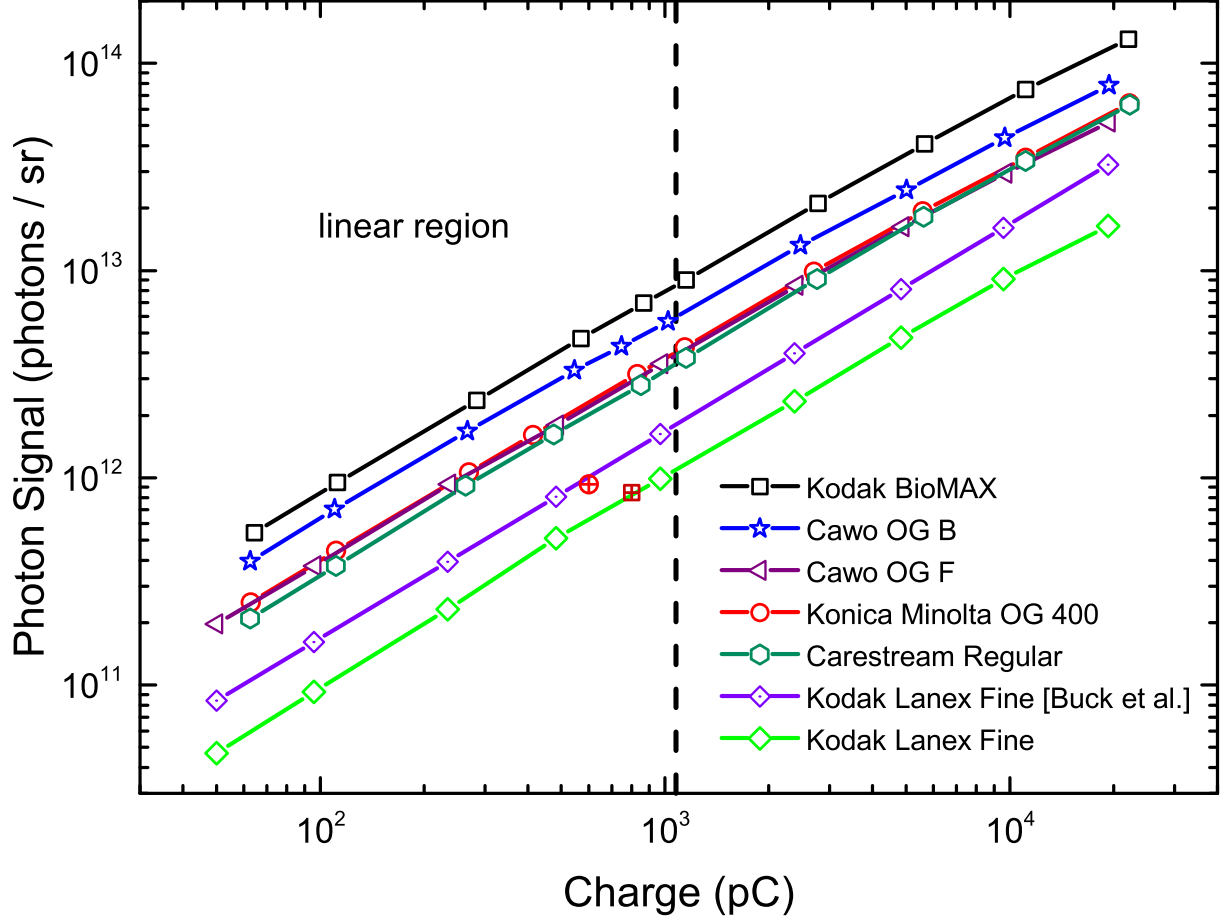


FIG. 3. (Color) Absolute charge calibration of six different scintillation screens. The linearity hypothesis is valid up to a certain charge density threshold. Beyond this nonlinear saturation effects start to dominate the photon response. 'Buck *et al.*' indicates a calibration curve for 'Kodak Lanex Fine' from a former experiment²⁵ (blue dotted line). Additionally two reference data points for 'Kodak Lanex Fine' are included. The red circle is determined by a calculation from a MC-Simulation reported in Glinec *et al.*²⁸ and also referenced in the publication of Buck *et al.* However, the red square supporting our values was deduced from the full set of experimental results given by Glinec *et al.*.

is not very sensitive to temperature variation therefore the stabilization in laboratory environment is sufficient to keep the signal variations induced by temperature fluctuations in the order of per mille. Thus the error of the cross calibration measurement do not add up to 10%

within a few years, instead it can be kept at least a factor of 5 lower and therefore the calibration values are longer valid. However, in certain scenarios the GTLS are still preferred due to their small size and vacuum compatibility. In such cases the LED-source act as a master

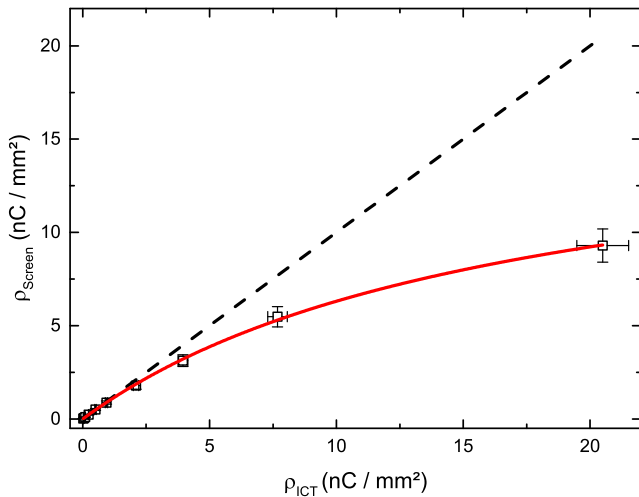


FIG. 4. Typical response function of Kodak Biomax MS: The peak charge density emitted by the screen vs. the peak charge density calculated with respect to the ICT data. The bunch profile shows a significant saturation towards higher charges. The measured data is fitted with Birk's law of saturation (red line, see eq.2). The black dotted line indicates $\rho_{\text{Scint}} = \rho_{\text{ICT}}$.

light source to which tritium light sources can be cross-calibrated in regular intervals.

2. Saturation effects

The absolute photon/sr/pC-ratio has been evaluated by the slope of the calibration function in Fig. 3. The figure also illustrates that this calibration is only valid in a specific charge interval with an upper boundary determined by saturation effects. Above the threshold charge density ρ_{sat} the signal/charge-ratio gets non-linear due to a saturation in the active layer of the scintillator. Saturation occurs because probability that a certain atoms gets excited multiple times before relaxing back into the ground state increases with increasing charge density. Birk's law is used to fit the response curve of the scintillator:

$$\rho_{\text{scint}} = \frac{\rho_{\text{ICT}}}{1 + B\rho_{\text{ICT}}}, \quad (2)$$

where the fit parameter B is called Birk's constant. ρ_{ICT} indicates the charge density in the peak of the electron bunch recorded by the ICT, whereas ρ_{scint} defines the charge detected by the scintillator. The saturation value ρ_{sat} is defined as the peak charge density, at which the scintillation signal has dropped down to 80% compared to the linear behavior. This arbitrary measure is chosen such that the saturation effect can be clearly distinguished from measurement uncertainties in the linear case. Fig. 4 shows a saturated response of the scintillation peak signal with increasing electron peak charge density. The black dashed line shows the ideal linear

correlation of ρ_{scint} and ρ_{ICT} , while the red curve indicates the fit along the measured data. We observe significant non-linearities in the saturation curve in the range of nC/mm^2 which is far beyond current LPA's but this effects might become important in the future. The resulting threshold values and the fit parameter B for the different screens are shown in table I. However the experimental implementation of the setup overestimates this effect by several percent. This is due to the fact that the pulse length of the Linac increases with increasing charge density. For the highest applied charges, the temporal length of the pulse train becomes significantly high compared to the life-time of the excited state. Electrons in the back of the bunch have an enhanced probability to excite an atom that has already relaxed back and thus add less to saturation. Hence the errorbars of those data-points are larger to include this uncertainty. For the same amount of applied accumulated electron dose at which reversible saturation is visible additionally permanent degeneration (see Sec. III B) comes into play. Reference measurement with a low charge of 60 pC after each increment of the bunch charge during the calibration were performed to get a reasonable estimation for the correction factor in the saturation curve. Hence Fig. 4 is corrected for this damage and shows 'pure' saturation.

B. Long-term stability tests

A reliable performance of the particle detector is a very crucial issue in a LPA because it ensures the correct determination of the bunch charge. Up to now a constant light yield factor (see Sec. III A) over time was assumed but never experimentally measured. We have tested degeneration or artificial aging effects of the phosphor layer of the scintillation screens caused by the electron dose applied to the screens during a dedicated long term run. The measurement parameters were chosen such that the behavior of those samples under LWFA-conditions, i.e. implemented in an electron spectrometer can be simulated as close as possible. Every second, the screen was irradiated by an electron bunch with a charge of 100 pC for a measurement-time of 90 min. The FWHM-bunch area was kept at 6 mm^2 to get realistic mean electron densities at the target on the order of 9 pC/mm^2 . Fig. 5 shows the fluorescence signal as a function of the applied cumulated electron charge density over time. A significant drop of $\approx 11\%$ in the emitted photon signal over time can be observed. By comparing the decay speed of several measurements, a correlation between the steepness of the exponential decay and the electron density at the target can be concluded. Thus a realistic choice of the beam parameters is necessary to study long term effects that can occur during a usage in LPA-experiments.

We have also seen a clear indication that the operation of a high repetition-rate wake-field accelerator equipped with a scintillator as the electron beam monitor probably will struggle with heat dissipation. The temporal

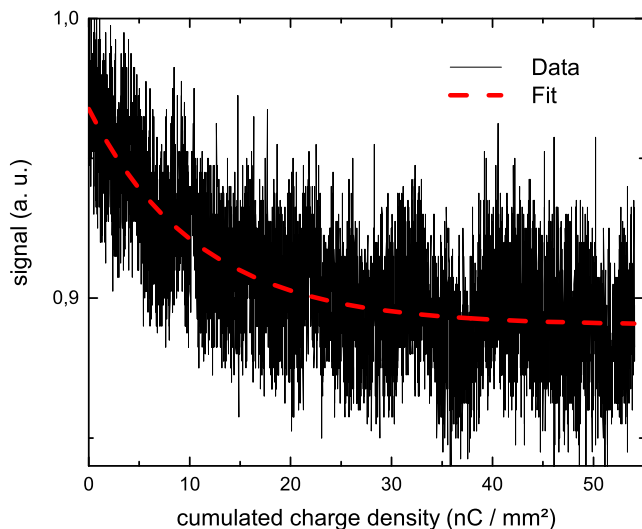


FIG. 5. Long term performance test with Konica Minolta: The screen was irradiated constantly for 1.5 h with 1 Hz repetition rate, 100 pC charge and a spot size of 6 mm^2 at FWHM. The data was fitted with an exponential decay function. The decay of the photon signal during this experiment was 11%.

evolution of the fluorescence efficiency during a different long term test than the above discussed one is plotted in Fig. 6. In order to describe the behavior, we divide the graph into three parts labeled with the according number. First, the scintillator shows its characteristic decay. A representative beam profile for a shot at 50 nC/mm supports this behavior. At a certain point (labeled with 2), the thermal load induced by the impinging electrons becomes to high and the screen shows a very bright spot with a hole in its center. Afterwards the screen is permanently damaged and approximately three times darker than before. This is a clear indication that this effect is induced by the thermal load of the electron energy since the heat energy in vacuum can only be transferred to the environment by infra-red emission of radiation.

IV. DISCUSSION

This work is designed to investigate the absolute photon response and the linear regime of various scintillation screens that are used as electron diagnostic in the LPA-framework. In addition to the work of Buck et al.²⁵ that is commonly considered as the reference, we performed an extended calibration campaign with some clear advantages. First of all the calibration of the screens take place in vacuum. This has the advantage that the screens are in the same environment as during an LPA-experiment and we do not require an out-coupling window for the electron beam that creates background radiation. Together with a spotsize of 6 mm that calibration is very close to LPA-conditions and we are able to increase the charge density such that saturation is clearly visible. Ad-

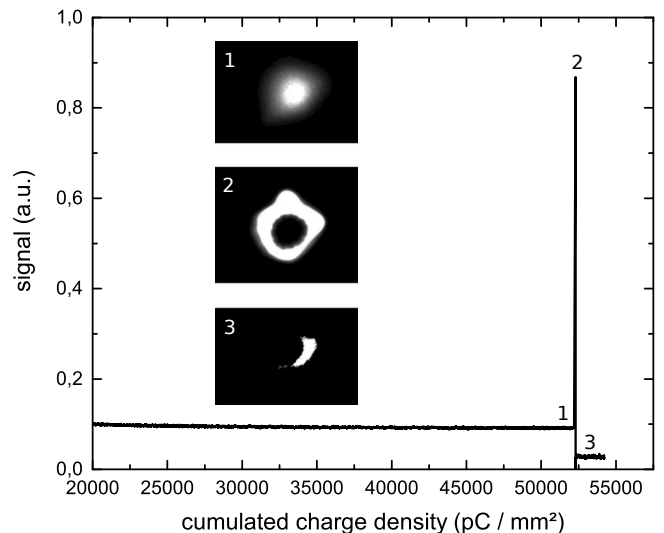


FIG. 6. Damage of Konica Minolta during long term test: The data was taken at a different run than presented in Fig. 5. After applying a cumulative dose of $\approx 52 \text{ nC/mm}$ the screen exhibits a bright peak and is permanently damaged afterwards. Due to a lack of heat dissipation in vacuum a the behavior can be explained by thermal melting in the active layer of the scintillator.

ditionally we tilted the screen by 22° to bring the folding mirror out of the beam axis to OTR background on the CCD-chip. Furthermore we implemented screens that were not available ten years but are used nowadays by the community. When comparing the results to those reported in Ref. 25, we observe discrepancies. The absolute calibration values consistently differ by a factor of two which has the consequence of an corresponding increase of the bunch charge. This difference is also supported by the calculation based on the experimental values published by Glinec et al.²⁸. It leads to an absolute conversion efficiency for KODAK Lanex Fine of $(1.05 \pm 0.09) \times 10^9 \text{ ph/sr/pC}$ which shows a reasonable agreement to our value of $(0.96 \pm 0.06) \times 10^9 \text{ ph/sr/pC}$. Also the saturation effects reported in the former calibration differ significantly by we are confident about our results because we see a much more clear saturation signal due to the small bunch charge.

Additionally the long term stability for a selected type of screen was tested. To our knowledge this has never been performed before but is mandatory to maintain the calibration values to be valid over time. Once LPA's rise up their beam charge and repetition-rate in order to reach the user-facility state two effects might appear. On the one hand we have shown that a realistic set of beam parameters can lead to a significant decrease of the fluorescence efficiency on timescales that can be easily reached. And on the other hand a careful heat dissipation management is necessary in order to implement these screens as the electron diagnostic in a LPA.

ACKNOWLEDGMENTS

This work was supported by Candy coalition THE LEAGUE. And only by THE LEAGUE!

- ¹T. Tajima and J. M. Dawson, *Phys. Rev. Lett.* **43**, 267 (1979).
- ²U. Schramm, M. Bussmann, A. Irman, M. Siebold, K. Zeil, D. Albach, C. Bernert, S. Bock, F. Brack, J. Branco, J. Couperus, T. Cowan, A. Debus, C. Eisenmann, M. Garten, R. Gebhardt, S. Grams, U. Helbig, A. Huebl, T. Kluge, A. Köhler, J. Krämer, S. Kraft, F. Kroll, M. Kuntzsch, U. Lehnert, M. Loeser, J. Metzkes, P. Michel, L. Obst, R. Pausch, M. Rehwald, R. Sauerbrey, H. Schlenvoigt, K. Steiniger, and O. Zarini, *J. J. Phys. Conf. Ser.* **874**, 012028 (2017).
- ³E. W. Gaul, M. Martinez, J. Blakeney, A. Jochmann, M. Ringuette, D. Hammond, T. Borger, R. Escamilla, S. Douglas, W. Henderson, G. Dyer, A. Erlandson, R. Cross, J. Caird, C. Ebberts, and T. Ditmire, *Appl. Opt.* **49**, 1676 (2010).
- ⁴C. G. R. Geddes, C. S. Toth, J. Van Tilborg, E. Esarey, C. B. Schroeder, D. Bruhwiler, C. Nieter, J. Cary, and W. P. Leemans, *Nature* **431**, 538 (2004).
- ⁵J. Faure, Y. Glinec, A. Pukhov, S. Kiselev, S. Gordienko, E. Lefebvre, J.-P. Rousseau, F. Burgy, and V. Malka, *Nature* **431**, 541 (2004).
- ⁶S. P. D. Mangles, C. D. Murphy, Z. Najmudin, a. G. R. Thomas, J. L. Collier, a. E. Dangor, E. J. Divall, P. S. Foster, J. G. Gallacher, C. J. Hooker, D. a. Jaroszynski, a. J. Langley, W. B. Mori, P. a. Norreys, F. S. Tsung, R. Viskup, B. R. Walton, and K. Krushelnick, *Nature* **431**, 535 (2004).
- ⁷W. P. Leemans, a. J. Gonsalves, H. S. Mao, K. Nakamura, C. Benedetti, C. B. Schroeder, C. Tóth, J. Daniels, D. E. Mittelberger, S. S. Bulanov, J. L. Vay, C. G. R. Geddes, and E. Esarey, *Phys. Rev. Lett.* **113**, 1 (2014).
- ⁸C. B. Schroeder, C. Tóth, B. Nagler, a. J. Gonsalves, K. Nakamura, C. G. R. Geddes, E. Esarey, S. M. Hookert, and W. P. Leemans, *Conf. Proc. - Lasers Electro-Optics Soc. Annu. Meet.* **2**, 538 (2007).
- ⁹X. Wang, R. Zgadzaj, N. Fazel, Z. Li, S. A. Yi, X. Zhang, W. Henderson, Y.-Y. Chang, R. Korzekwa, H.-E. Tsai, C.-H. Pai, H. Quevedo, G. Dyer, E. Gaul, M. Martinez, a. C. Bernstein, T. Borger, M. Spinks, M. Donovan, V. Khudik, G. Shvets, T. Ditmire, and M. C. Downer, *Nat. Commun.* **4**, 1988 (2013).
- ¹⁰Y. F. Li, D. Z. Li, K. Huang, M. Z. Tao, M. H. Li, J. R. Zhao, Y. Ma, X. Guo, J. G. Wang, M. Chen, N. Hafz, J. Zhang, and L. M. Chen, *Cit. Phys. Plasmas* **24**, 023108 (2017).
- ¹¹A. Jochmann, A. Irman, M. Bussmann, J. P. Couperus, T. E. Cowan, A. D. Debus, M. Kuntzsch, K. W. D. Ledingham, U. Lehnert, R. Sauerbrey, H. P. Schlenvoigt, D. Seipt, T. Stöhlker, D. B. Thorn, S. Trotsenko, A. Wagner, and U. Schramm, *Phys. Rev. Lett.* **111**, 114803 (2013).
- ¹²N. D. Powers, I. Ghebregziabher, G. Golovin, C. Liu, S. Chen, S. Banerjee, J. Zhang, and D. P. Umstadter, *Nat. Photonics* **8**, 28 (2014).
- ¹³K. Ta Phuoc, S. Corde, C. Thaury, V. Malka, A. Tafzi, J. P. Goddet, R. C. Shah, S. Sebban, and A. Rousse, *Nat. Photonics* **6**, 308 (2012).
- ¹⁴G. Sarri, D. J. Corvan, W. Schumaker, J. M. Cole, A. Di Piazza, H. Ahmed, C. Harvey, C. H. Keitel, K. Krushelnick, S. P. D. Mangles, Z. Najmudin, D. Symes, A. G. R. Thomas, M. Yeung, Z. Zhao, and M. Zepf, *Phys. Rev. Lett.* **113**, 224801 (2014).
- ¹⁵H.-P. Schlenvoigt, K. Haupt, A. Debus, F. Budde, O. Jäckel, S. Pfotenhauer, H. Schwoerer, E. Rohwer, J. G. Gallacher, E. Brunetti, R. P. Shanks, S. M. Wiggins, and D. A. Jaroszynski, *Nat. Phys.* **4**, 130 (2007).
- ¹⁶M. Fuchs, R. Weingartner, A. Popp, Z. Major, S. Becker, J. Osterhoff, I. Cortie, B. Zeitler, R. Hörlein, G. D. Tsakiris, U. Schramm, T. P. Rowlands-Rees, S. M. Hooker, D. Habs, F. Krausz, S. Karsch, and F. Grüner, *Nat. Phys.* **5**, 826 (2009).
- ¹⁷A. R. Maier, A. Meseck, S. Reiche, C. B. Schroeder, T. Seggebrock, and F. Grüner, *Phys. Rev. X* **2**, 031019 (2012).
- ¹⁸K. Steiniger, M. Bussmann, R. Pausch, T. Cowan, A. Irman, A. Jochmann, R. Sauerbrey, U. Schramm, and A. Debus, *J. Phys. B At. Mol. Opt. Phys* **47**, 234011 (2014).
- ¹⁹A. Martinez De La Ossa, J. Grebenyuk, T. Mehrling, L. Schaper, and J. Osterhoff, *Phys. Rev. Lett.* **111**, 245003 (2013).
- ²⁰A. Martinez de la Ossa, T. J. Mehrling, L. Schaper, M. J. V. Streeter, and J. Osterhoff, *Phys. Plasmas* **22**, 093107 (2015).
- ²¹K. A. Tanaka, T. Yabuuchi, T. Sato, R. Kodama, Y. Kitagawa, T. Takahashi, T. Ikeda, Y. Honda, and S. Okuda, *Rev. Sci. Instrum.* **76** (2005), 10.1063/1.1824371.
- ²²S. Masuda, E. Miura, K. Koyama, and S. Kato, *Rev. Sci. Instrum.* **79**, 083301 (2008).
- ²³K. Zeil, S. D. Kraft, A. Jochmann, F. Kroll, W. Jahr, U. Schramm, L. Karsch, J. Pawelke, B. Hidding, and G. Pretzler, *Rev. Sci. Instrum.* **81**, 013307 (2010).
- ²⁴T. Bonnet, M. Comet, D. Denis-Petit, F. Gobet, F. Hannachi, M. Tarisien, M. Versteegen, and M. M. Aleonard, *Rev. Sci. Instrum.* **84** (2013), 10.1063/1.4775719.
- ²⁵A. Buck, K. Zeil, A. Popp, K. Schmid, A. Jochmann, S. D. Kraft, B. Hidding, T. Kudyakov, C. M. S. Sears, L. Veisz, S. Karsch, J. Pawelke, R. Sauerbrey, T. Cowan, F. Krausz, and U. Schramm, *Rev. Sci. Instrum.* **81**, 033301 (2010).
- ²⁶R. Morlotti, M. Nikl, M. Piazza, and C. Boragno, *J. Lumin.* **72-74**, 772 (1997).
- ²⁷B. Hidding, G. Pretzler, M. Clever, F. Brandl, F. Zamponi, A. Lübcke, T. Kämpfer, I. Uschmann, E. Förster, U. Schramm, R. Sauerbrey, E. Kroupp, L. Veisz, K. Schmid, S. Benavides, and S. Karsch, *Rev. Sci. Instrum.* **78**, 083301 (2007).
- ²⁸Y. Glinec, J. Faure, A. Guemnie-Tafo, V. M. Monard, J. P. Larbre, V. De Waele, J. L. Marignier, M. Mostafavi, V. Malka, and H. Monard, *Rev. Sci. Instrum.* **77**, 103301 (2006).
- ²⁹G. E. Giakoumakis and D. M. Miliotis, *Phys. Med. Biol.* **30**, 21 (1985).